Informatics

# Flower State Classification for Watering System

DIPLOMARBEIT

zur Erlangung des akademischen Grades

**Diplom-Ingenieur**

im Rahmen des Studiums

**Software Engineering & Internet Computing**

eingereicht von

**Tobias Eidelpes, BSc**
Matrikelnummer 01527193

an der Fakultät für Informatik
der Technischen Universität Wien

Betreuung: Ao.Univ.-Prof. Dr. Horst Eidenberger

Wien, 20. Februar 2023

| Tobias Eidelpes | Horst Eidenberger |
|---|---|

TU WIEN Informatics

# Flower State Classification for Watering System

DIPLOMA THESIS

submitted in partial fulfillment of the requirements for the degree of

**Diplom-Ingenieur**

in

**Software Engineering & Internet Computing**

by

**Tobias Eidelpes, BSc**
Registration Number 01527193

to the Faculty of Informatics

at the TU Wien

Advisor: Ao.Univ.-Prof. Dr. Horst Eidenberger

Vienna, 20th February, 2023

Tobias Eidelpes Horst Eidenberger

# Erklärung zur Verfassung der Arbeit

Tobias Eidelpes, BSc

Hiermit erkläre ich, dass ich diese Arbeit selbständig verfasst habe, dass ich die verwendeten Quellen und Hilfsmittel vollständig angegeben habe und dass ich die Stellen der Arbeit – einschließlich Tabellen, Karten und Abbildungen –, die anderen Werken oder dem Internet im Wortlaut oder dem Sinn nach entnommen sind, auf jeden Fall unter Angabe der Quelle als Entlehnung kenntlich gemacht habe.

Wien, 20. Februar 2023

Tobias Eidelpes

# Danksagung

Ihr Text hier.

# Acknowledgements

Enter your text here.

# Kurzfassung

Ihr Text hier.

# Abstract

Enter your text here.

# Contents

CHAPTER 1

# Evaluation

The following sections contain a detailed evaluation of the model in various scenarios. First, we present metrics from the training phases of the constituent models. Second, we employ methods from the field of Explainable Artificial Intelligence (XAI) such as Gradient-weighted Class Activation Mapping (Grad-CAM) to get a better understanding of the models' abstractions. Finally, we turn to the models' aggregate performance on the test set and discuss whether the initial goals set by the problem description have been met or not.

## 1.1 Object Detection

The object detection model was pre-trained on the COCO [LMB+15] dataset and fine-tuned with data from the Open Images Dataset (OID) [KRA+20] in its sixth version. Since the full OID dataset contains considerably more classes and samples than would be feasibly trainable on a small cluster of GPUs, only images from the two classes *Plant* and *Houseplant* have been downloaded. The samples from the Houseplant class are merged into the Plant class because the distinction between the two is not necessary for our model. Furthermore, the OID contains not only bounding box annotations for object detection tasks, but also instance segmentations, classification labels and more. These are not needed for our purposes and are omitted as well. In total, the dataset consists of 91479 images with a roughly 85/5/10 split for training, validation and testing, respectively.

### 1.1.1 Training Phase

The object detection model was trained for 300 epochs on 79204 images with 284130 ground truth labels. The weights from the best-performing epoch were saved. The model's fitness for each epoch is calculated as the weighted average of mAP@0.5 and mAP@0.5:0.95:

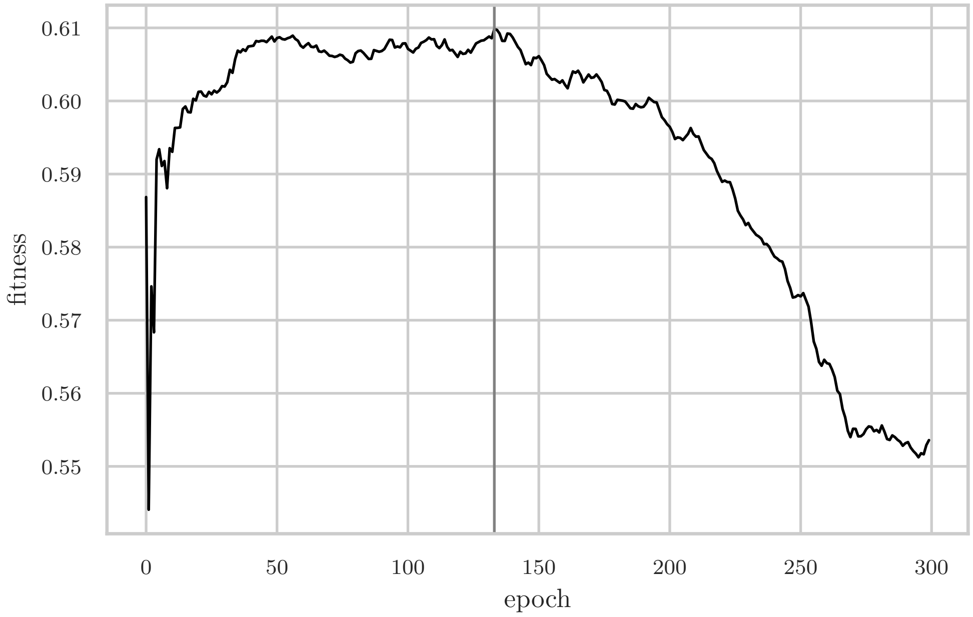

Figure 1.1: Object detection model fitness for each epoch calculated as in equation 1.1. The vertical gray line at 133 marks the epoch with the highest fitness.

$$f_{epoch} = 0.1 \cdot \mathsf{mAP@}0.5 + 0.9 \cdot \mathsf{mAP@}0.5{:}0.95 \tag{1.1}$$

Figure 1.1 shows the model's fitness over the training period of 300 epochs. The gray vertical line indicates the maximum fitness of 0.61 at epoch 133. The weights of that epoch were frozen to be the final model parameters. Since the fitness metric assigns the mAP at the higher range the overwhelming weight, the mAP@0.5 starts to decrease after epoch 30, but the mAP@0.5:0.95 picks up the slack until the maximum fitness at epoch 133. This is an indication that the model achieves good performance early on and continues to gain higher confidence values until performance deteriorates due to overfitting.

Overall precision and recall per epoch are shown in figure 1.2. The values indicate that neither precision nor recall change materially during training. In fact, precision starts to decrease from the beginning, while recall experiences a barely noticeable increase. Taken together with the box and object loss from figure 1.3, we speculate that the pre-trained model already generalizes well to plant detection because one of the categories in the COCO [LMB$^+$15] dataset is *potted plant*. Any further training solely impacts the confidence of detection, but does not lead to higher detection rates. This conclusion is supported by the increasing mAP@0.5:0.95 until epoch 133.

Further culprits for the flat precision and recall values may be found in bad ground truth data. The labels from the OID are sometimes not fine-grained enough. Images

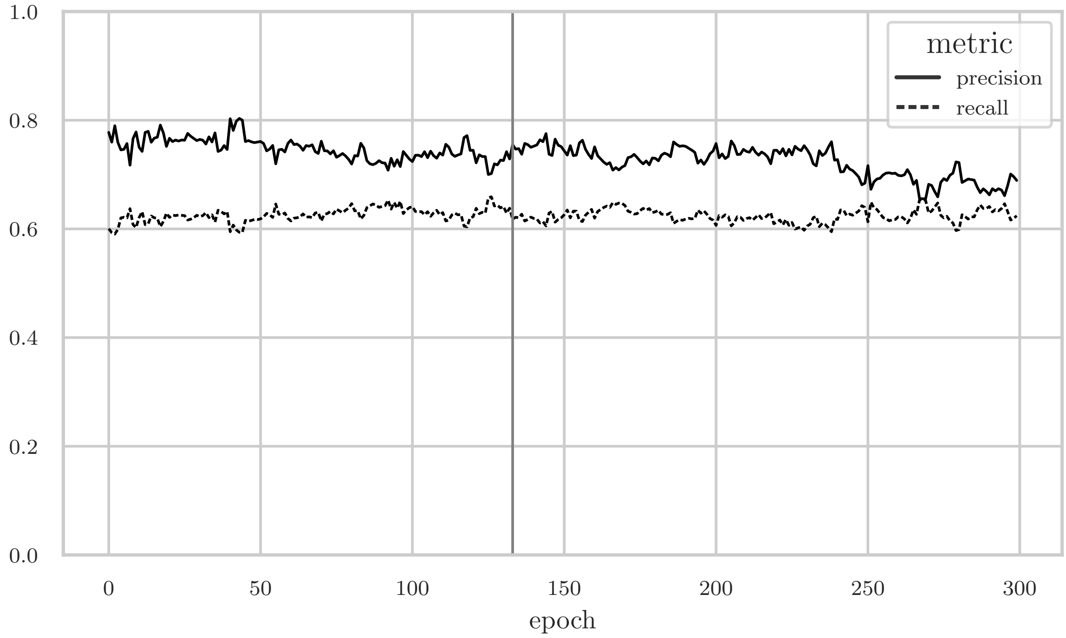

Figure 1.2: Overall precision and recall during training for each epoch. The vertical gray line at 133 marks the epoch with the highest fitness.

which contain multiple individual—often overlapping—plants are labeled with one large bounding box instead of multiple smaller ones. The model recognizes the individual plants and returns tighter bounding boxes even if that is not what is specified in the ground truth. Therefore, it is prudent to limit the training phase to relatively few epochs in order to not penalize the more accurate detections of the model. The smaller bounding boxes make more sense considering the fact that the cutout is passed to the classifier in a later stage. Smaller bounding boxes help the classifier to only focus on one plant at a time and to not get distracted by multiple plants in potentially different stages of wilting.

The box loss decreases slightly during training which indicates that the bounding boxes become tighter around objects of interest. With increasing training time, however, the object loss increases, indicating that less and less plants are present in the predicted bounding boxes. It is likely that overfitting is a cause for the increasing object loss from epoch 40 onward. Since the best weights as measured by fitness are found at epoch 133 and the object loss accelerates from that point, epoch 133 is probably the correct cutoff before overfitting occurs.

### 1.1.2 Test Phase

Of the 91479 images around 10% were used for the test phase. These images contain a total of 12238 ground truth labels. Table 1.1 shows precision, recall and the harmonic mean of both (F1-score). The results indicate that the model errs on the side of sensitivity

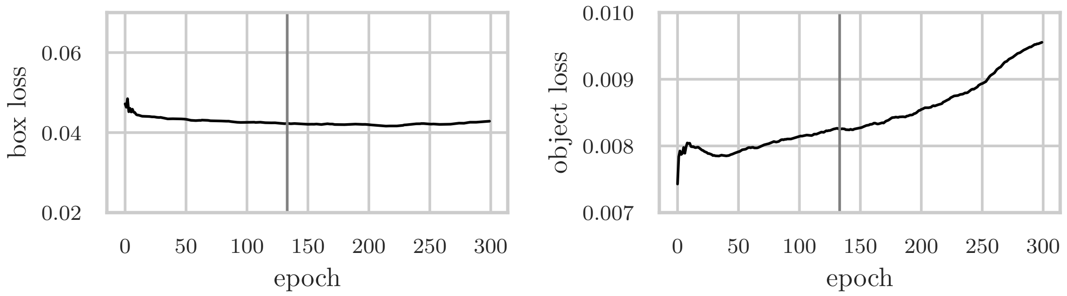

Figure 1.3: Box and object loss measured against the validation set of 3091 images and 4092 ground truth labels. The class loss is omitted because there is only one class in the dataset and the loss is therefore always zero.

because recall is higher than precision. Although some detections are not labeled as plants in the dataset, if there is a labeled plant in the ground truth data, the chance is high that it will be detected. This behavior is in line with how the model's detections are handled in practice. The detections are drawn on the original image and the user is able to check the bounding boxes visually. If there are wrong detections, the user can ignore them and focus on the relevant ones instead. A higher recall will thus serve the user's needs better than a high precision.

| | Precision | Recall | F1-score | Support |
|---|---|---|---|---|
| Plant | 0.547571 | 0.737866 | 0.628633 | 12238.0 |

Table 1.1: Precision, recall and F1-score for the object detection model.

Figure 1.4 shows the Average Precision (AP) for the Intersection over Union (IOU) thresholds of 0.5 and 0.95. Predicted bounding boxes with an IOU of less than 0.5 are not taken into account for the precision and recall values of table 1.1. The lower the detection threshold, the more plants are detected. Conversely, a higher detection threshold leaves potential plants undetected. The precision-recall curves confirm this behavior because the area under the curve for the threshold of 0.5 is higher than for the threshold of 0.95 (0.66 versus 0.41). These values are combined in COCO's [LMB$^+$15] main evaluation metric which is the AP averaged across the IOU thresholds from 0.5 to 0.95 in 0.05 steps. This value is then averaged across all classes and called mean average precision (mAP). The object detection model achieves a state-of-the-art mAP of 0.5727 for the *Plant* class.

## 1.2 Classification

The classifier receives cutouts from the object detection model and determines whether the image shows a stressed plant or not. To achieve this goal, we trained a Residual Neural Network (ResNet) [HZR$^+$16] on a dataset of 452 images of healthy and 452

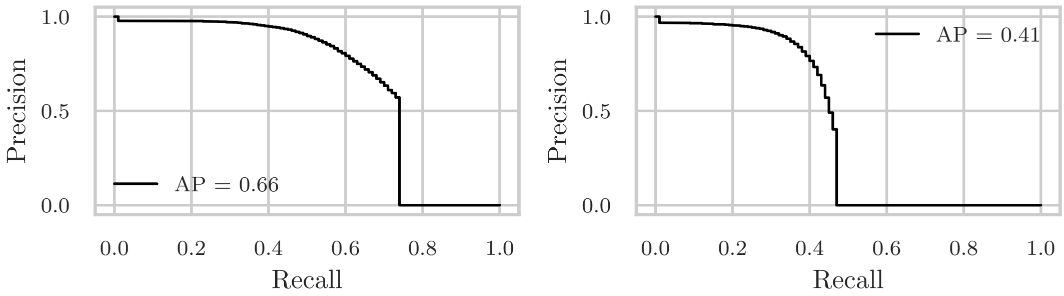

Figure 1.4: Precision-recall curves for IOU thresholds of 0.5 and 0.95. The AP of a specific threshold is defined as the area under the precision-recall curve of that threshold. The mAP across IOU thresholds from 0.5 to 0.95 in 0.05 steps mAP@0.5:0.95 is 0.5727.

stressed plants. We chose the ResNet architecture due to its popularity and ease of implementation as well as its consistently high performance on various classification tasks. While its classification speed in comparison with networks optimized for mobile and edge devices (e.g. MobileNet) is significantly lower, the deeper structure and the additional parameters are necessary for the fairly complex task at hand. Furthermore, the generous time budget for object detection *and* classification allows for more accurate results at the expense of speed. The architecture allows for multiple different structures, depending on the amount of layers. The smallest one has 18 and the largest 152 layers with 34, 50 and 101 in-between. The larger networks have better accuracy in general, but come with trade-offs regarding training and inference time as well as required space. The 50 layer architecture (ResNet50) is adequate for our use case.

### 1.2.1 Training Phase

The dataset was split 85/15 into training and validation sets. The images in the training set were augmented with a random crop to arrive at the expected image dimensions of 224 pixels. Additionally, the training images were modified with a random horizontal flip to increase the variation in the set and to train a rotation invariant classifier. All images, regardless of their membership in the training or validation set, were normalized with the mean and standard deviation of the ImageNet [DDS+09] dataset, which the original ResNet model was pre-trained with. Training was done for 50 epochs and the best-performing model as measured by validation accuracy was selected as the final version.

Figure 1.5 shows accuracy and loss on the training and validation sets. There is a clear upwards trend until epoch 20 when validation accuracy and loss stabilize at around 0.84 and 0.3, respectively. The quick convergence and resistance to overfitting can be attributed to the model already having robust feature extraction capabilities.

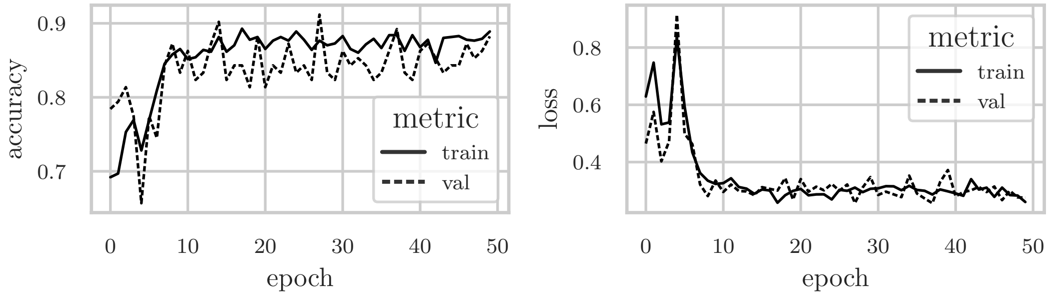

Figure 1.5: Accuracy and loss during training of the classifier. The model converges quickly, but additional epochs do not cause validation loss to increase, which would indicate overfitting. The maximum validation accuracy of 0.9118 is achieved at epoch 27.

### 1.2.2 Class Activation Maps

Neural networks are notorious for their black-box behavior, where it is possible to observe the inputs and the corresponding outputs, but the stage in-between stays hidden from view. Models are continuously developed and deployed to aid in human decision-making and sometimes supplant it. It is, therefore, crucial to obtain some amount of interpretability of what the model does *inside* to be able to explain why a decision was made in a certain way. The research field of XAI gained significance during the last few years because of the development of new methods to peek inside these black boxes.

One such method, Class Activation Mapping (CAM) [ZKL+15], is a popular tool to produce visual explanations for decisions made by Convolutional Neural Networks (CNNs). Convolutional layers essentially function as object detectors as long as no fully-connected layers perform the classification. This ability to localize regions of interest which play a significant role in the type of class the model predicts, can be retained until the last layer and used to generate activation maps for the predictions.

A more recent approach to generating a CAM via gradients is proposed by Selvaraju et al. [SCD+20]. Their Grad-CAM approach works by computing the gradient of the feature maps of the last convolutional layer with respect to the specified class. The last layer is chosen because the authors find that “[...] Grad-CAM maps become progressively worse as we move to earlier convolutional layers as they have smaller receptive fields and only focus on less semantic local features.” [SCD+20, p.5]

Turning to our classifier, figure 1.6 shows the CAMs for *healthy* and *stressed.* While the regions of interest for the *healthy* class lie on the healthy plant, the *stressed* plant is barely considered and mostly rendered as background information (blue). Conversely, when asked to explain the inputs to the *stressed* classification, the regions of interest predominantly stay on the thirsty as opposed to the healthy plant. In fact, the large hanging leaves play a significant role in determining the class the image belongs to. This is an additional data point confirming that the model focuses on the *right* parts of the image during classification.

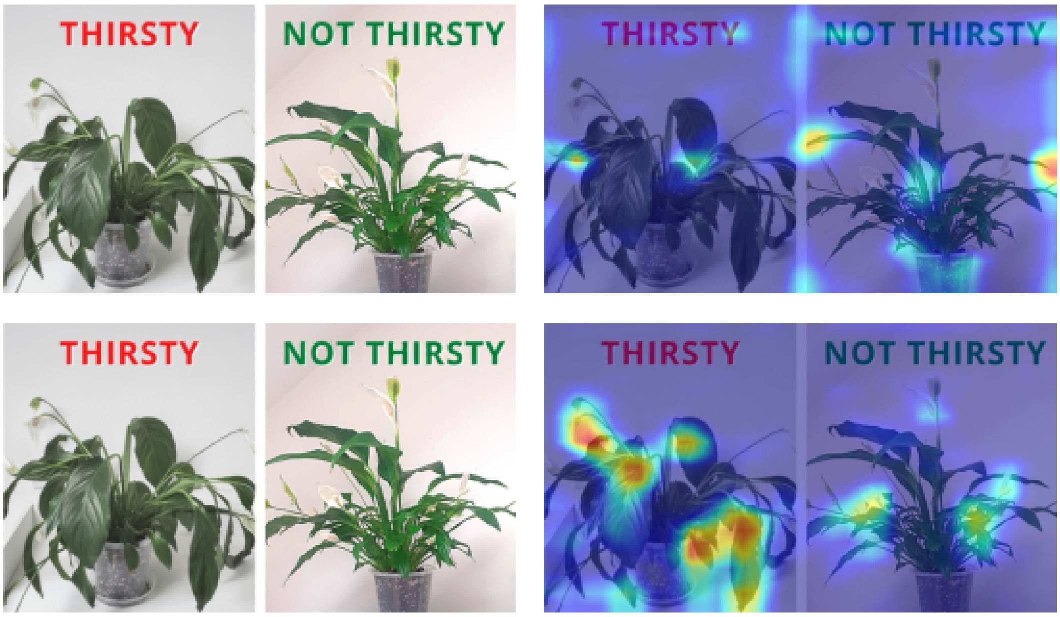

Figure 1.6: The top left image shows the original image of the same plant in a stressed (left) and healthy (right) state. In the top right image, the CAM for the class *healthy* is laid over the original image. The classifier draws its conclusion mainly from the healthy plant, which is indicated by the red hot spots around the tips of the plant. The bottom right image shows the CAM for the *stressed* class. The classifier focuses on the hanging leaves of the thirsty plant. The image was classified as *stressed* with a confidence of 70%.

## 1.3 Aggregate Model

In this section we turn to the evaluation of the aggregate model. We have confirmed the performance of the constituent models: the object detection and the classification model. It remains to evaluate the complete pipeline from gathering detections of potential plants in an image and forwarding them to the classifier to obtaining the results as either healthy or stressed with their associated confidence scores.

The test set contains 640 images which were obtained from a google search using the terms *thirsty plant*, *wilted plant* and *stressed plant*. Images which clearly show one or multiple plants with some amount of visible stress were added to the dataset. Care was taken to include plants with various degrees of stress and in various locations and lighting conditions. The search not only provided images of stressed plants, but also of healthy plants due to articles, which describe how to care for plants, having a banner image of healthy plants. The dataset is biased towards potted plants which are commonly put on display in western households. Furthermore, many plants, such as succulents, are sought after for home environments because of their ease of maintenance. Due to their inclusion in the dataset and how they exhibit water stress, the test set nevertheless contains a

| | Precision | Recall | F1-score | Support |
|---|---|---|---|---|
| Healthy | 0.824 | 0.745 | 0.783 | 662.0 |
| Stressed | 0.707 | 0.783 | 0.743 | 488.0 |
| micro avg | 0.769 | 0.761 | 0.765 | 1150.0 |
| macro avg | 0.766 | 0.764 | 0.763 | 1150.0 |
| weighted avg | 0.775 | 0.761 | 0.766 | 1150.0 |

Table 1.2: Precision, recall and F1-score for the aggregate model.

wide variety of scenarios.

After collecting the images, the aggregate model was run on them to obtain initial bounding boxes and classifications for ground truth labeling. Letting the model do the work beforehand and then correcting the labels allowed to include more images in the test set because they could be labeled more easily. Additionally, going over the detections and classifications provided a comprehensive view on how the models work and what their weaknesses and strengths are. After the labels have been corrected, the ground truth of the test set contains 662 bounding boxes of healthy plants and 488 of stressed plants.

Table 1.2 shows precision, recall and the F1-score for both classes *Healthy* and *Stressed*. Both precision and recall are balanced and the F1-score is high. Unfortunately, these values do not take the accuracy of bounding boxes into account and thus have only limited expressive power.

Figure 1.7 shows the precision and recall curves for both classes at different IOU thresholds. The left plot shows the AP for each class at the threshold of 0.5 and the right one at 0.95. The mAP is 0.6226 and calculated across all classes as the median of the IOU thresholds from 0.5 to 0.95 in 0.05 steps. The difference between mAP@0.5 and mAP@0.95 is fairly small which indicates that the bounding boxes encapsulate the objects of interest well. The cliffs at around 0.77 (left) and 0.7 (right) happen at a detection threshold of 0.5. The classifier's last layer is a softmax layer which necessarily transforms the input into a probability of showing either a healthy or stressed plant. If the probability of an image showing a healthy plant is below 0.5, it is no longer classified as healthy but as stressed. The threshold for discriminating the two classes lies at the 0.5 value and is therefore the cutoff for either class.

Overall, we believe that the aggregate model shows sufficient predictive performance to be deployed in the field. The detections are accurate, especially for potted plants, and the classification into healthy and stressed is robust.

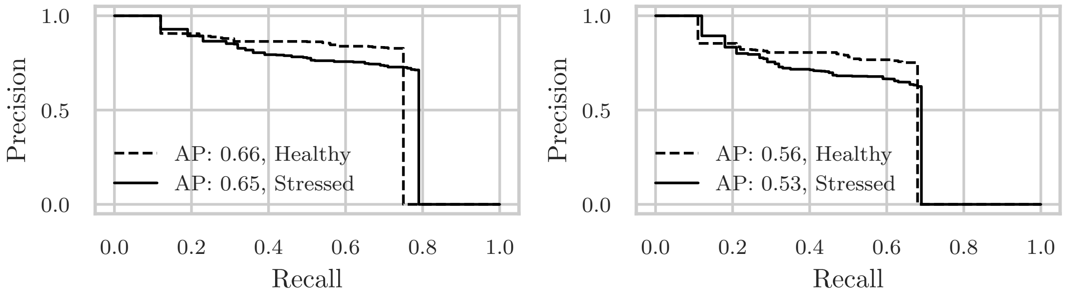

Figure 1.7: Precision-recall curves for IOU thresholds of 0.5 and 0.95. The AP of a specific threshold is defined as the area under the precision-recall curve of that threshold. The mAP across IOU thresholds from 0.5 to 0.95 in 0.05 steps `mAP@0.5:0.95` is 0.6226.

# List of Figures

# List of Tables

# List of Algorithms

# Acronyms

**AP** Average Precision. 4, 5, 8

**CAM** Class Activation Mapping. 6, 9

**CNN** Convolutional Neural Network. 6

**Grad-CAM** Gradient-weighted Class Activation Mapping. 1, 6

**IOU** Intersection over Union. 4, 5, 8

**mAP** mean average precision. 4, 5, 8

**OID** Open Images Dataset. 1, 2

**ResNet** Residual Neural Network. 4, 5

**XAI** Explainable Artificial Intelligence. 1, 6

# Bibliography

[DDS+09] Jia Deng, Wei Dong, Richard Socher, Li-Jia Li, Kai Li, and Li Fei-Fei. ImageNet: A large-scale hierarchical image database. In *2009 IEEE Conference on Computer Vision and Pattern Recognition.* 2009 IEEE Conference on Computer Vision and Pattern Recognition, pages 248–255, June 2009. DOI: 10.1109/CVPR.2009.5206848.

[HZR+16] Kaiming He, Xiangyu Zhang, Shaoqing Ren, and Jian Sun. Deep Residual Learning for Image Recognition. In *2016 IEEE Conference on Computer Vision and Pattern Recognition (CVPR).* 2016 IEEE Conference on Computer Vision and Pattern Recognition (CVPR), pages 770–778, June 2016. DOI: 10.1109/CVPR.2016.90.

[KRA+20] Alina Kuznetsova, Hassan Rom, Neil Alldrin, Jasper Uijlings, Ivan Krasin, Jordi Pont-Tuset, Shahab Kamali, Stefan Popov, Matteo Malloci, Alexander Kolesnikov, Tom Duerig, and Vittorio Ferrari. The Open Images Dataset V4: Unified image classification, object detection, and visual relationship detection at scale. *International Journal of Computer Vision*, 128(7):1956–1981, July 2020. DOI: 10.1007/s11263-020-01316-z.

[LMB+15] Tsung-Yi Lin, Michael Maire, Serge Belongie, Lubomir Bourdev, Ross Girshick, James Hays, Pietro Perona, Deva Ramanan, C. Lawrence Zitnick, and Piotr Dollár. Microsoft COCO: Common Objects in Context. February 20, 2015. DOI: 10.48550/arXiv.1405.0312. preprint.

[SCD+20] Ramprasaath R. Selvaraju, Michael Cogswell, Abhishek Das, Ramakrishna Vedantam, Devi Parikh, and Dhruv Batra. Grad-CAM: Visual Explanations from Deep Networks via Gradient-based Localization. *International Journal of Computer Vision*, 128(2):336–359, February 2020. DOI: 10.1007/s11263-019-01228-7.

[ZKL+15] Bolei Zhou, Aditya Khosla, Agata Lapedriza, Aude Oliva, and Antonio Torralba. Learning Deep Features for Discriminative Localization. December 13, 2015. DOI: 10.48550/arXiv.1512.04150. preprint.